nature energy

ARTICLES

PUBLISHED: 22 AUGUST 2016 | ARTICLE NUMBER: 16126 | DOI: 10.1038/NENERGY.2016.126

Steam generation under one sun enabled by a floating structure with thermal concentration

George Ni[1], Gabriel Li[1], Svetlana V. Boriskina[1], Hongxia Li[2], Weilin Yang[2], TieJun Zhang[2] and Gang Chen[1]*

Harvesting solar energy as heat has many applications, such as power generation, residential water heating, desalination, distillation and wastewater treatment. However, the solar flux is diffuse, and often requires optical concentration, a costly component, to generate the high temperatures needed for some of these applications. Here we demonstrate a floating solar receiver capable of generating 100 °C steam under ambient air conditions without optical concentration. The high temperatures are achieved by using thermal concentration and heat localization, which reduce the convective, conductive and radiative heat losses. This demonstration of a low-cost and scalable solar vapour generator holds the promise of significantly expanding the application domain and reducing the cost of solar thermal systems.

The sun is a promising and abundant source of renewable energy that can potentially solve many of society's challenges. Solar thermal technologies, that is, the conversion of the sunlight to thermal energy, are being developed for many applications, such as power generation, domestic water heating, desalination, and other industrial processes[1–7]. Steam and vapour generation is often desired in these applications, but the dilute solar flux (1,000 W m^{-2}) does not provide enough power per unit area of the absorber to reach the required high temperatures and to compensate for the large latent heat of water vaporization. Optical concentrators, such as parabolic troughs, heliostats and lenses, can concentrate the ambient solar flux tens or even thousands of times to achieve high temperatures[8–12]. Plasmonic nanoparticles with absorption and scattering cross-sections exceeding their geometrical cross-sections have been recently developed and applied for direct solar steam generation[13–24], but they typically require optical concentration of 10–1,000× for steam generation However, optical concentrators are expensive (US$200 m^{-2})[25], often accounting for a major portion of the capital cost of solar thermal systems[8,11,26]. In addition, they require support structures and access to electrical energy to track the sun. Although optical concentration is at present necessary for applications that require high temperatures, such as concentrated solar power generation, solar thermal technologies that reduce or completely eliminate the reliance on optical concentration would have better market penetration. Worldwide, the use of non-concentrated solar thermal power (∼200 GW)[27] outnumbers the use of concentrated solar thermal power (∼5 GW).

We recently demonstrated solar steam generation under low (≤10×) optical concentration using a floating graphite-based two-layer solar absorber[28]. This structure localized the solar heat generation to the evaporation surface of a body of water, instead of wastefully heating the entire body of water. The structure's top layer absorbed the solar flux, while the bottom layer limited conduction of the generated heat to the underlying body of water. This resulted in very high steam generation efficiencies of up to 85%. However, to reach 100 °C for steam generation, a solar flux of 10 kW m^{-2}, 10 times the normal sun (1,000 W m^{-2}), was needed by optical concentration. Several other groups have looked into the role of surface chemistry in aiding water delivery and thermal insulation of the bottom layer[20], incorporating plasmonic or carbon-based absorption layers[29–33], and using other cheap and abundant materials[34,35]. These studies have achieved relatively high evaporation efficiencies, but relied on optical concentration to boost the evaporation temperatures and achieve such efficiencies. For example, Ito *et al.*[29] used a concentration of 9× to achieve steam generation. To reach the boiling point without optical concentration, solar receivers must be designed to suppress parasitic heat losses from the absorber surface.

Here, we demonstrate water boiling and steam generation under unconcentrated ambient solar flux in a receiver open to the ambient. The receiver is constructed of a variety of low-cost and commercially available materials, utilizing a combination of spectral selectivity of the solar absorber, thermal insulation, and in-plane thermal concentration. By varying the thermal concentration, the receiver can generate saturated steam at 100 °C, or low-temperature vapour at high efficiencies (64%). The ability to boil water under ambient sunlight holds promise for significant cost reduction of existing solar thermal systems while opening up new applications such as desalination, wastewater treatment, and sterilization.

Generating high-temperature vapour with low solar flux

Achieving steam generation using the ambient solar flux (1,000 W m^{-2}), or one sun, requires significant reduction of the heat losses from the receiver. Figure 1a shows the heat transfer processes involved in a floating solar steam generator, including radiative and convective heat loss to the ambient and conductive and radiative heat loss to the underlying water. The net evaporation rate $\dot{m}$ can be expressed as

$$\dot{m}h_{fg} = A\alpha q_{solar} - A\varepsilon\sigma\left(T^4 - T_\infty^4\right) - Ah\left(T - T_\infty\right) - Aq_{water} \quad (1)$$

where h_{fg} is the latent heat, A the surface area of the absorber facing the sun, α the solar absorptance, q_{solar} the solar flux, ε the emittance

[1]Department of Mechanical Engineering, Massachusetts Institute of Technology, 77 Massachusetts Avenue, Cambridge, Massachusetts 02139, USA.
[2]Department of Mechanical and Materials Engineering, Masdar Institute of Science and Technology, PO Box 54224, Abu Dhabi, United Arab Emirates.
*e-mail: gchen2@mit.edu

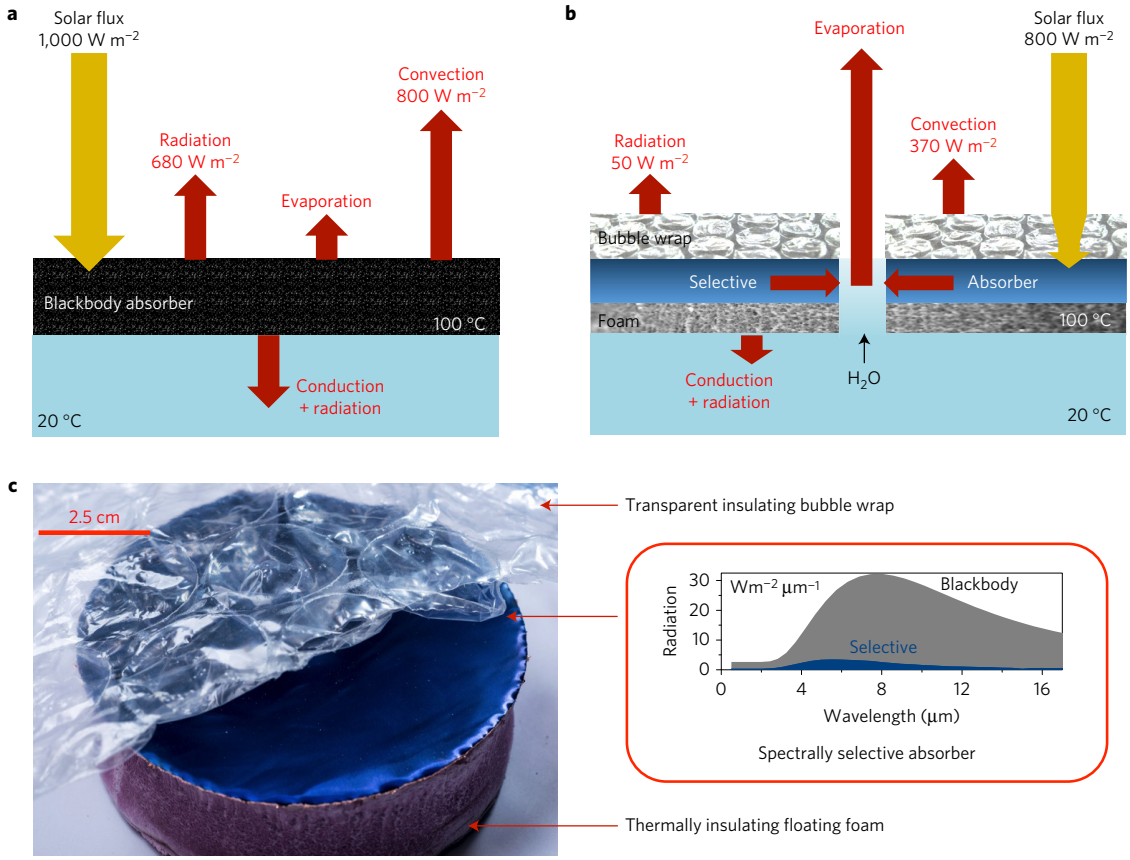

Figure 1 | Operating principles of steam generation at one sun. a, Energy balance and heat transfer diagram for a blackbody solar receiver operating at 100 °C. The 1,000 W m^{-2} delivered by the ambient solar flux is not enough to sustain the heat losses, and a 100 °C equilibrium temperature cannot be reached. **b**, Energy balance and heat transfer in the developed one-sun, ambient steam generator (OAS). **c**, A photograph of the OAS composed of a commercial spectrally selective coating on copper to suppress radiative losses and to thermally concentrate heat to the evaporation region. The bubble wrap cover transmits sunlight, and minimizes convective losses. Slots are cut in the bubble wrap to allow steam to escape. Thermal foam insulates the hot selective absorber from the cool underlying water, and floats the entire structure. The inset compares thermal radiative losses at 100 °C from a blackbody and the spectrally selective absorber.

of the absorbing surface, σ the Stefan–Boltzmann constant, h the convection heat transfer coefficient, and q_{water} the heat flux to the underlying water, including conduction and radiation. Assuming a blackbody absorber with T = 100 °C, the minimum temperature needed for boiling water at ambient conditions, and T_∞ = 20 °C, the radiative heat loss to the ambient is 680 W m^{-2}. Taking a natural convection heat transfer coefficient of 10 W m^{-2} K, the convective heat loss is 800 W m^{-2}. These two loss channels alone exceed the incoming solar flux of 1,000 W m^{-2}, and there is additional heat loss to the underlying water by conduction and radiation.

The large mismatch between water's latent heat of vaporization h_{fg} (2.26 MJ kg^{-1} at 100 °C) and the ambient solar flux imposes another challenge. Even without any parasitic energy losses, the maximum mass flux generated by the ambient solar flux is $\dot{m}/A = q_{solar}/h_{fg} = 4.4 \times 10^{-4}$ kg m^{-2} s, according to equation (1). Our past studies[28] have shown that the mass evaporation rate of water at 100 °C can be an order of magnitude higher (up to 4.3×10^{-3} kg m^{-2} s).

Figure 1b shows several strategies we used to overcome the above challenges to achieve continuous steam generation under one sun and even lower solar flux as shown later. First, we replace the blackbody absorber with a spectrally selective absorber, which has high solar absorptance α and low thermal emittance ε (Fig. 1c). Spectrally selective absorbers strongly absorb sunlight, but emit very little radiative heat. They are already widely used in domestic solar hot water systems[36,37], and allow evacuated solar hot water tubes to be heated to over 100 °C under stagnation conditions[38]. However, these solar hot water heating systems are not designed for steam generation or evaporation from open bodies of water. Second, we use thermal insulation on both top and bottom surfaces of the absorber to reduce convective loss to air as well as conductive and radiative heat losses to the water underneath. Finally, to overcome the mismatch between the latent heat of vaporization and the ambient solar flux, we use thermal concentration, by conducting the absorbed heat into the evaporation area, which is smaller than the absorber surface area.

One-sun, ambient steam generator

Figure 2 shows the lab-scale one-sun, ambient steam generator (OAS), which contains three main components. First, a spectrally selective solar absorber is used, consisting of a cermet (BlueTec eta plus) coated on a copper sheet. Second, a thermal insulator was constructed from a polystyrene foam disk. Last, a convective cover was made from a sheet of large transparent bubble wrap. We use a variety of low-cost commercial materials to construct the solar receiver, and we believe even cheaper materials can be substituted for intended applications, as discussed later; one example is using alternative selective coatings.

The spectrally selective absorber (Fig. 2a) solar absorptance (α = 0.93) and emittance at 100 °C (ε = 0.07) were both measured

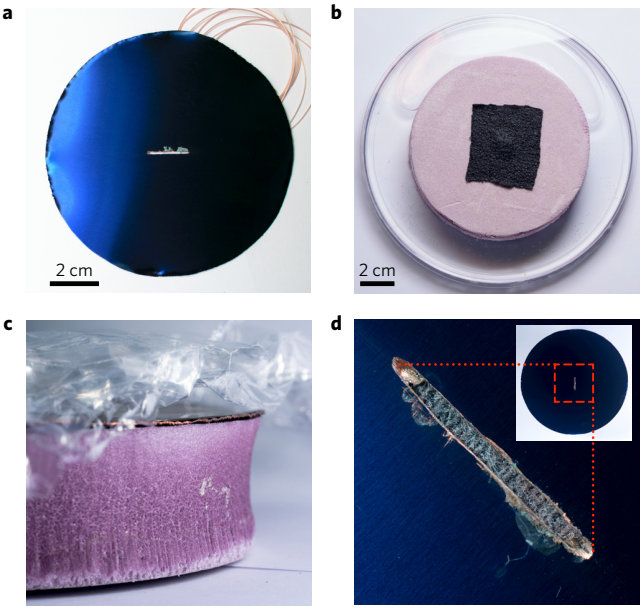

Figure 2 | One-sun, ambient steam generator. a, The selective absorber consists of a commercially available cermet-coated copper substrate. **b**, The insulation foam serves to float the entire structure on a body of water, and limits the thermal conduction and radiation to the cool water underneath. The dark fabric in the centre hides a fabric wick, which tunnels through the foam to the underlying water. The fabric draws water through the foam. The clear container surrounding the foam holds water, and has a cap to prevent extraneous evaporation. **c**, The three layers of the OAS, from top to bottom: bubble wrap, selective absorber and thermally insulating foam. **d**, The evaporation slot, which reveals the dark fabric underneath. The fabric serves to deliver water, but also increases the evaporation area. The inset shows where the evaporation slot is cut.

and are shown in the Supplementary Methods. The polystyrene foam shown in Fig. 2b,c serves to float the entire structure on a body of water, and is a thermal insulator (k =~ 0.03 W m^{-1} K). A channel was drilled through the foam, and a hydrophilic cotton wick threaded through. This wick used capillary forces to deliver water to the absorber. A sheet of cotton fabric (Fig. 2b) was placed above the wick on the foam to increase the evaporative area. Figure 2d shows an evaporation slot cut into a 10 cm diameter selective absorber, to allow for water vapour to escape. The slot was varied in length (1 mm width) to control the operating temperature of the receiver. For smaller thermal concentrations, 2–3 slots were made in a concentrated cluster (~5–10 mm separation).

A sheet of transparent bubble wrap (Fig. 2c) was placed on top of the selective absorber to minimize the convective losses. The solar transmittance τ_{bubble} of the bubble wrap was measured to be 80%. Though the bubble wrap reduces the solar power transmitted and absorbed by the absorber surface, it also reduces the convective heat losses. The result is a net improvement in the OAS performance.

Laboratory experiments

The lab-scale OAS performance was first characterized in a laboratory environment (Supplementary Methods). A solar simulator was used to supply solar flux (1,000 W m^{-2}), and a balance was used to measure the real-time mass loss of the receiver and water supply. The selective absorber temperature and vapour temperature were measured (Fig. 3a) as a function of the thermal concentration C_{therm}, the ratio of the total illumination area to the evaporation area. The vapour temperature closely tracks the selective absorber temperature. The maximum steam temperature reached was 98 °C (Fig. 3b), achieved when ~0.1% of the surface is devoted to evaporation (C_{therm} = 1,300×). The steam temperature was directly measured by the thermocouple in this case, using a small vapour chamber. The kink near t = 300 s clearly indicates boiling limiting further temperature rise of the solar receiver, despite the measured vapour temperature not exactly reaching 100 °C due to the rapid cooling of vapour. Figure 3c shows the mass change as a function of time while generating 80 °C vapour. These figures show the receiver reached steady-state operation in roughly 5 min, clearly demonstrating continuous steam generation under 1 sun illumination.

The solar vapour generation efficiency was defined as a ratio of enthalpy change in the generated vapour divided by the total incoming solar flux:

$$\eta_{thermal} = \frac{\dot{m} h_{fg}}{q_{solar} A} \quad (2)$$

where $\dot{m}$ is the instantaneous mass change due to evaporation, h_{fg} is the enthalpy change of liquid water to vapour, q_{solar} is the solar flux per area, and A is the total area of the receiver. Figure 3d shows the receiver efficiencies at different operating temperatures. The lines in Fig. 3d were obtained by using a heat transfer model of the OAS, which is discussed below.

Generating steam outdoors

An outdoor experiment using natural sunlight validated the ability of the OAS to generate steam in real conditions, where factors such as varying incident solar flux and wind can greatly hinder receiver performance. The OAS was placed on the roof of MIT, at noontime for all experiments. Thermocouples were used to measure the selective absorber temperature, and a thermal pyranometer used to measure the incident solar flux on a horizontal surface, known as the global horizontal irradiance. Figure 4 shows the selective absorber temperatures and solar fluxes during the two experimental runs (6 August and 17 September 2015). Based on the lab data, when the selective absorber reaches 100 °C, steam is generated.

Figure 4a shows a measurement on a sunny day with roaming cloud cover, which caused the solar flux to vary dramatically (~200–1,000 W m^{-2}). The temperature measurements show that the selective absorber is capable of recovering its peak operating temperature (>95 °C) within minutes. Figure 4b shows a situation where the sun is more constant, but at a lower position in the sky due to seasonal variation. This lower sky position reduces the amount of solar flux incident on a horizontal surface (~750 W m^{-2}). These experiments demonstrate the ability of the solar receiver to rapidly reach 100 °C temperatures during periods of low and varying solar flux, such as during non-summer months and cloudy days.

Modelling

We carried out modelling to gain insights into the present experiment and future performance (Supplementary Notes 1). A key requirement for efficient thermal concentration is limiting the temperature drop along the surface of the selective absorber. A large temperature drop reduces efficiency, and indicates significant heat loss compared to the heat conduction to the evaporation region. We used a simple fin model to justify that the temperature throughout the selective absorber is nearly uniform, consistent with our measurements. We incorporate this isothermal assumption into the isothermal model. We also carried out COMSOL simulations to determine the sidewall losses in the lab-scale experimental OAS. The results are plotted in Fig. 3d.

The isothermal model is used to predict the achievable performance of a large-scale OAS where the side wall heat loss is negligible. Such a large-scale OAS is expected to have repeating patterns of evaporation slots, thus maintaining the isothermal

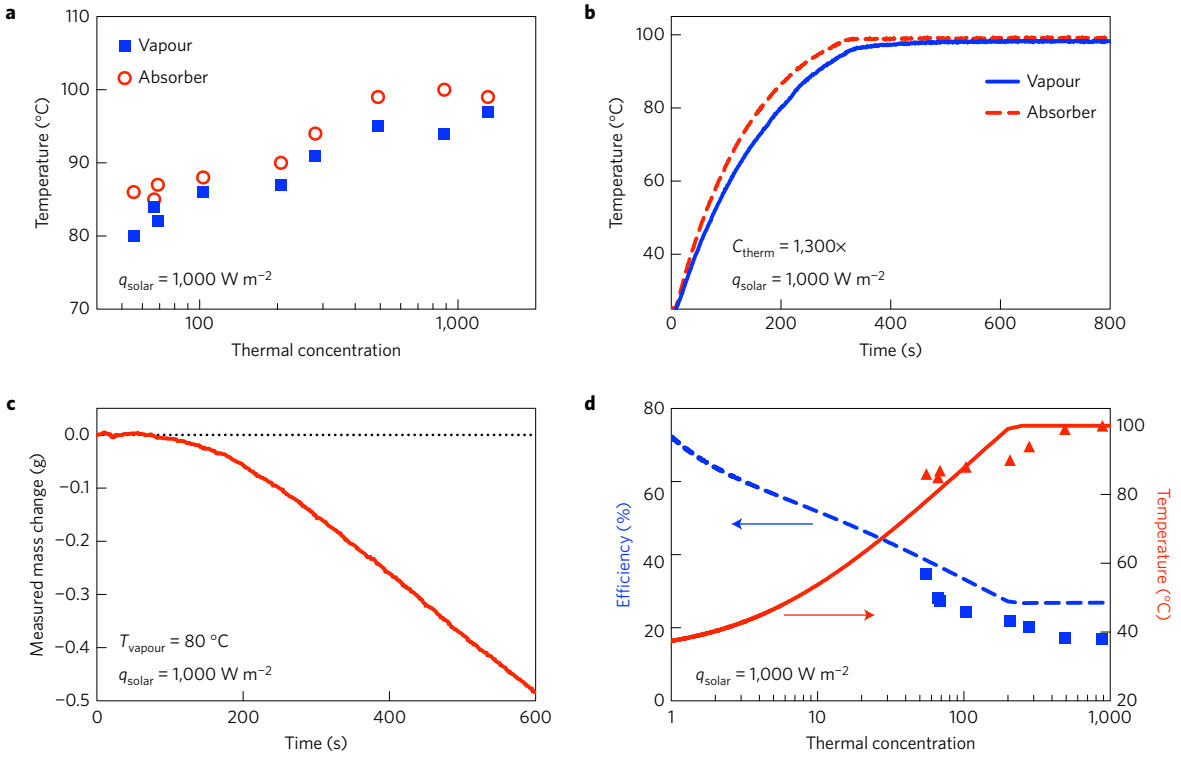

Figure 3 | Vapour generation experimental results. a, Steady-state vapour and selective absorber temperatures measured as a function of the thermal concentration used. The evaporation slots were varied in size to control the operating temperature. **b**, Vapour and selective absorber temperatures versus time at a thermal concentration of 1,300×. The vapour temperature was directly measured with a small vapour chamber that was placed over the evaporation area. The kink in temperature rise is due to phase change. **c**, Mass change over time, when the produced vapour temperature is 80 °C. The OAS quickly reaches a steady-state condition. **d**, Efficiency of the receiver versus thermal concentration. The dots are measurements, and the lines are computed by using the OAS heat transfer model (Supplementary Notes 1).

absorber. Figure 5a shows the achievable vapour temperatures and efficiencies predicted while under 1,000 W m^{-2} illumination. The maximum temperature reached was 100 °C with a thermal concentration around 200×. The thermal concentration required to generate steam is higher than the optical concentration reported in previous experiments[28,29], but is significantly easier to implement. Higher thermal concentration yielded lower evaporation efficiency, due to reduced evaporation area. However, once the steam generation temperature has been reached (100 °C), increasing thermal concentration does not change the efficiency much, due to phase change limiting any further temperature rise. Theoretically, superheating may occur at higher thermal concentrations, leading to increased heat losses and lower efficiency. These scenarios are not included in the model, as they are not observed in the thermal concentrations tested in this study. At low thermal concentration with large evaporation area, the efficiency of the system is higher, but the vapour temperature generated is low due to the higher evaporation rates. Based on the results of our modelling, two useful receiver configurations were identified: one for high-temperature (100 °C) vapour generation, and another for high-efficiency evaporation (C_{therm} = 1×).

Figure 5b shows the predicted performance of the OAS at different solar fluxes (obtained by using the model in Supplementary Notes 1, coefficients in Supplementary Notes 2) at C_{therm} = 1× and C_{therm} = 1,000×. This illustrates the ability of the OAS to generate steam throughout the day, when the sun is at different positions in the sky. The temperature plateau indicates phase change limiting the temperature rise of the OAS, consistent with measurements. Figure 5c shows a sensitivity analysis of the maximum operating temperature of the OAS to the transmittance of the bubble wrap and absorptance of the selective surface ($\tau_{bubble}\alpha$). The thermal concentration was set to 1,000×. The receiver can generate steam with $\tau_{bubble}\alpha >\sim 0.4$, with increasing efficiency at higher $\tau_{bubble}\alpha$. At lower $\tau_{bubble}\alpha$ the receiver is generating vapour via evaporation. Figure 5d shows sensitivity of the maximum operating temperature to the receiver emittance. It reveals that the OAS can generate steam even if the selective solar absorber has significantly poorer optical properties than the one used in our system. This suggests that the most expensive component, the selective absorber, can be made more cheaply than what was used in this paper.

Discussion

Another area for optimization of the receiver is the evaporation slot design. Understanding the dominating resistances in the evaporation process can give us key insights into how to improve the design. Using Schrage's model[39], an upper limit for evaporative heat transfer coefficient is estimated to be on the order of 10^7 W m^{-2} K (Supplementary Notes 7). This is five orders of magnitude higher than the coefficients measured in this work (~500 W m^{-2} K, Supplementary Notes 2). This suggests that the overall evaporation rate is limited by vapour diffusion through air, not vapour formation at the liquid-air interface. In support of this conclusion, the evaporation heat transfer coefficient increased ~10× over those in a previous work[28], probably due to the difference in the system geometry. The system in ref. 26 had an evaporation surface with a large planar area, resulting in one-dimensional (1D) vapour diffusion away from the liquid. In contrast, OAS evaporation areas are better approximated by lines, enabling 2D vapour diffusion, and resulting in larger evaporation heat transfer coefficients. Additional evaporation experiments were conducted to determine the size

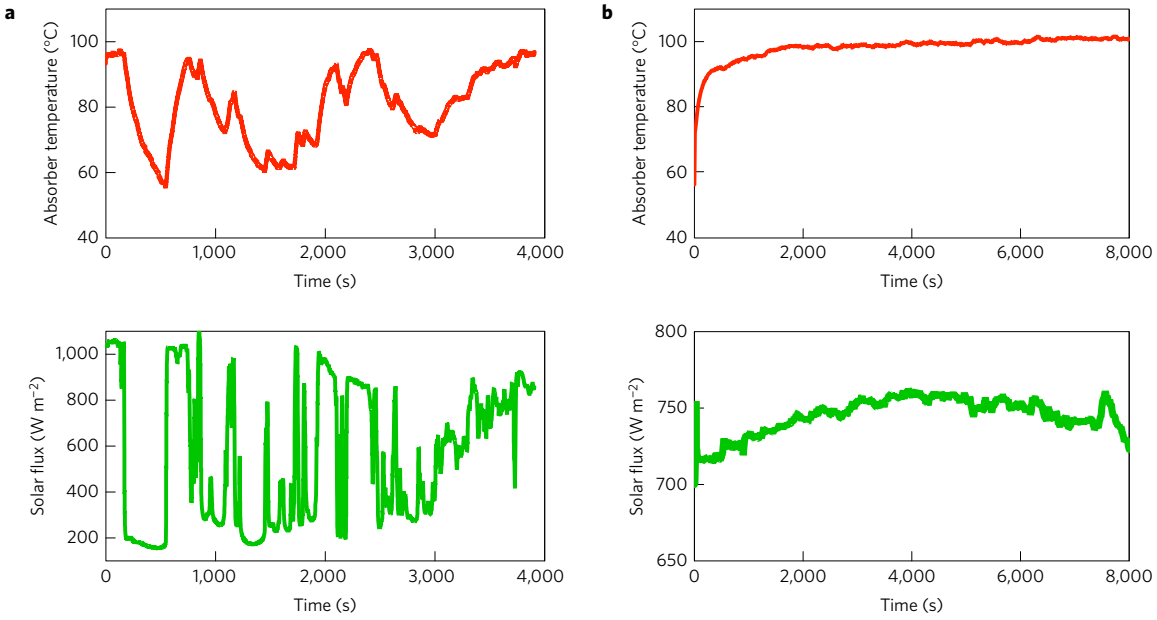

Figure 4 | Outdoor performance under natural sunlight. Temperature measurements of the OAS in outdoor conditions on two separate dates: 6 August 2015 (**a**) and 17 September 2015 (**b**). Panel **a** demonstrates the ability of the OAS to rapidly reach peak operating temperature on cloudy days, whereas panel **b** demonstrates its ability to generate steam during low solar flux days (non-summer seasons). For each experiment, the thermal concentration was 1,000×.

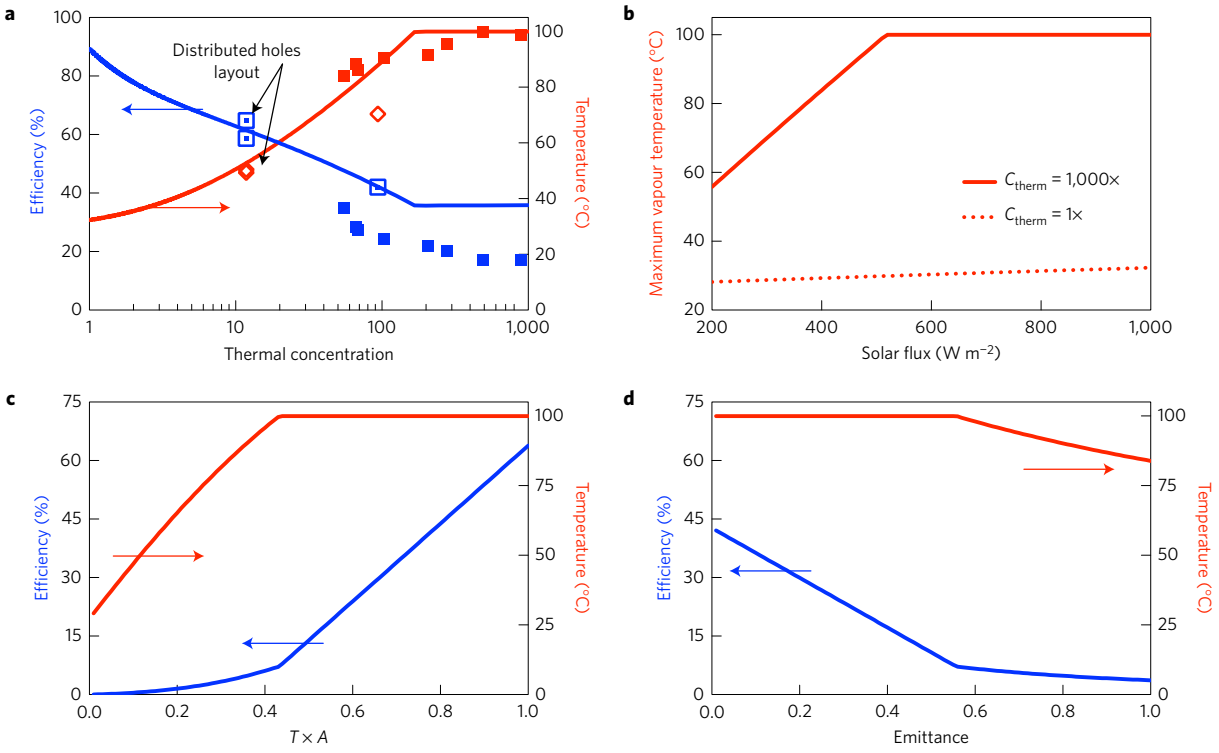

Figure 5 | Analysis of a large-scale OAS performance. a, The achievable performance of the receiver using an isothermal absorber approximation (see Supplementary Notes 1). Unless otherwise stated, the OAS optical properties were ε = 0.07, α = 0.93 and τ_{bubble} = 0.8. The solar flux is 1,000 W m^{-2} and the thermal concentration 1,000×. The open data points indicate the measured performance of a high-efficiency version of the OAS with distributed holes. The lines represent the predicted achievable performance of a large OAS with negligible side losses. **b**, Performance at various solar fluxes for low and high thermal concentrations. **c**, Sensitivity of efficiency and maximum temperature to the product of bubble wrap transmittance and selective surface absorptance. Thermal concentration is 1,000×. **d**, Sensitivity of the receiver to emittance ε, which affects radiative losses. Transmittance and absorptance have a larger effect on efficiency than emittance. Absorbers with significantly poorer optical properties than our selective surface can be used to generate steam, suggesting cheaper material substitutions in future designs.

effect of evaporation areas. Smaller circular evaporation areas improved the per area evaporation rate dramatically, up to 10× increase for a 36× reduction in area (Supplementary Notes 7). Further analysis using COMSOL determined that closely space evaporation areas improved efficiency (Supplementary Notes 4).

Even though the present single slot configuration has a higher mass transfer coefficient than ref. 26, the mass flux is much smaller due to reduced area of evaporation. One way to improve evaporation efficiency is to distribute numerous smaller circular slots for 3D vapour diffusion, while preserving the thermal concentration ratio for the overall area. This strategy maximizes the volume of air for vapour diffusion per distributed circular slot, enhancing the overall evaporation rate. Two additional OAS were created utilizing distributed circular slots, and generated low-temperature vapour at much higher efficiencies (Fig. 5a). The highest efficiency reached was 71% at 12× thermal concentration (64% after subtracting the evaporation under dark conditions). The effective evaporation heat transfer coefficient for the total receiver area was higher than in ref. 26 (29 W m^{-2} K versus 25 W m^{-2} K), and the OAS achieved this with much smaller actual evaporation areas.

Demonstration of continuous direct steam generation under the one-sun condition opens many potential applications, such as distillation and sterilization in remote locations. By pressurizing the system, one can potentially use the approach to generate superheated steam—for power conversion using water or other organic working fluids. The floating structure also has potential for solar desalination when the generated vapour is collected. Solar stills have been used for thousands of years, but have remained underutilized due to their low-efficiency (30–45%) and relatively high cost[40–42]. The basic design of the solar still uses a black-bottomed water basin to absorb the incoming solar flux. In such a configuration, radiative losses from the hot water are the largest source of losses, and cannot be avoided. Our approach significantly reduces the radiative loss, as well as the convective losses. There are several examples of floating solar stills in the literature[43,44], but these are simply basic single-effect solar stills made to float on the ocean. Hence, the cost and efficiency are expected to be similar or worse than conventional solar stills. The OAS can achieve higher efficiencies than an uncovered solar still using alternative receivers[45]. Furthermore, when placed in a solar still, the OAS efficiency can be higher, due to better insulation from the environment. In addition, the floating structure will enable direct deployment on water surfaces, such as over a bay, hence reducing system complexity and cost.

We have shown that thermal concentration can be a more cost-effective approach to solar steam generation than optical concentration. The OAS is estimated to cost ∼US$6 m^{-2}, based on available bulk pricing of materials, and we expect the cost can be reduced down to ∼US$2 m^{-2}. The manufacturing processes for final product are expected to be roll-to-roll, and should be of low cost. The cost of tracking optical concentrators can be as high as US$200 m^{-2}, and much of the prior literature on solar vapour generation has not included the optical losses due to inefficient concentration of the full solar flux, both diffuse and direct. Taking these details into account, the OAS can generate steam at ∼5% the cost of optically concentrating approaches (Supplementary Notes 5).

Further study in fouling of the OAS is needed, though the decoupling of the optical absorber from the phase change surface is an advantage. The cotton wick is a small fraction of the solar absorber, and its fouling will not affect the solar absorption. Accumulated salt may be sufficiently rejected overnight if used in an ocean. The wick is also easy to replace, being a small component. Overall, the ability of the OAS to generate high-temperature steam without relying on bulky and costly concentrating optics opens up many new possibilities for solar thermal energy harvesting.

Methods

The selective absorber's solar absorptance was measured using an ultraviolet–visible spectrophotometer (Agilent Cary 5000) with an included integrating sphere, and the emittance was measured using a Fourier transform infrared (FTIR) spectrometer (Thermo Nicolet 5700) with a Pike Technologies mid-IR integrating sphere.

The receiver performance experiments were conducted in the lab using a solar simulator (ScienceTech, SS-1.6K) outputting simulated solar flux at 1 kW m^{-2} (1 sun). The solar flux intensity was measured using a thermopile (Newport, 818P-001-12) connected to a power meter (Newport, 1918-C). Because the solar flux varies with the beam spot location, and the thermopile detector is smaller in area than the solar receiver, the maximum-recorded solar flux is regarded as the actual constant solar flux for the efficiency measurements. This under-reports the vapour generation efficiency up to 5%, based on the actual variation observed in solar flux. A 10 cm aperture is used to minimize the amount of extraneous solar flux striking the receiver. The mass of the water loss is measured using a lab balance with 1 mg resolution (A&D, FX300i), and calibrated to weights higher than the solar receiver. Before illuminating the solar receiver, the evaporation in dark conditions was measured for 10 min. The dark-evaporation rate was subtracted from the solar-illuminated evaporation rate, which was measured for 30 min at steady-state conditions.

The evaporation mass loss of the receiver under dark conditions was measured, and subtracted from the measured mass loss under solar illumination. Due to a low mass flux, the produced vapour quickly mixes with the surrounding air and cools. The temperature of the produced vapour was measured by touching a thermocouple to the cotton evaporation surface. For measurement of the highest temperature, a vapour chamber was constructed to collect the generated steam. In this case, the thermocouple was suspended in air to directly measure the steam temperature. The selective absorber's temperature was measured as well via a thermocouple attached under the copper substrate.

The rooftop measurements were conducted using the A&D FX300i balance to measure water loss, and a Hukseflux LP-02 thermal pyranometer to measure the intensity of the sun. Thermocouples (Omega Engineering, K-type, 40 gauge insulated) were used to measure the temperature of the selective absorber.

Received 10 February 2016; accepted 20 July 2016; published 22 August 2016

References

1. Dalvi, V. H., Panse, S. V. & Joshi, J. B. Solar thermal technologies as a bridge from fossil fuels to renewables. *Nat. Clim. Change* **5**, 1007–1013 (2015).
2. Shannon, M. A. *et al.* Science and technology for water purification in the coming decades. *Nature* **452**, 301–310 (2008).
3. Narayan, G. P. *et al.* The potential of solar-driven humidification-dehumidification desalination for small-scale decentralized water production. *Renew. Sustain. Energy Rev.* **14**, 1187–1201 (2010).
4. Elimelech, M. & Phillip, W. A. The future of seawater desalination: energy, technology, and the environment. *Science* **333**, 712–717 (2011).
5. Li, C., Goswami, Y. & Stefanakos, E. Solar assisted sea water desalination: a review. *Renew. Sustain. Energy Rev.* **19**, 136–163 (2013).
6. Tiwari, G. N., Singh, H. N. & Tripathi, R. Present status of solar distillation. *Sol. Energy* **75**, 367–373 (2003).
7. Phelan, P., Taylor, R., Adrian, R., Prasher, R. & Otanicar, T. *Nanoparticle Heat Transfer Fluid Flow* (CRC Press, 2012).
8. Weinstein, L. A. *et al.* Concentrating solar power. *Chem. Rev.* **115**, 12797–12838 (2015).
9. Boriskina, S. V. *et al.* Roadmap on optical energy conversion. *J. Opt.* **18**, 073004 (2016).
10. Jenkins, D. *et al.* Solar concentration of 50,000 achieved with output power approaching 1 kW. *J. Sol. Energy Eng.* **118**, 141–145 (1996).
11. Reif, J. H. & Alhalabi, W. Solar-thermal powered desalination: its significant challenges and potential. *Renew. Sustain. Energy Rev.* **48**, 152–165 (2015).
12. Montes, M. J., Abánades, A. & Martínez-Val, J. M. Performance of a direct steam generation solar thermal power plant for electricity production as a function of the solar multiple. *Sol. Energy* **83**, 679–689 (2009).
13. Neumann, O. *et al.* Solar vapor generation enabled by nanoparticles. *ACS Nano* **7**, 29–42 (2013).
14. Neumann, O. *et al.* Nanoparticle-mediated, light-induced phase separations. *Nano Lett.* **15**, 7880–7885 (2015).
15. Neumann, O. *et al.* Compact solar autoclave based on steam generation using broadband light-harvesting nanoparticles. *Proc. Natl Acad. Sci. USA* **110**, 11677–11681 (2013).
16. Liu, Y. *et al.* A bioinspired, reusable, paper-based system for high-performance large-scale evaporation. *Adv. Mater.* **27**, 2768–2774 (2015).
17. Wang, Z. *et al.* Evaporation: bio-inspired evaporation through plasmonic film of nanoparticles at the air-water interface. *Small* **10**, 3233–3233 (2014).

18. Boriskina, S. V., Ghasemi, H. & Chen, G. Plasmonic materials for energy: from physics to applications. *Mater. Today* **16**, 375–386 (2013).
19. Tian, L. *et al.* Plasmonic biofoam: a versatile optically active material. *Nano Lett.* **16**, 609–616 (2015).
20. Yu, S. *et al.* The impact of surface chemistry on the performance of localized solar-driven evaporation system. *Sci. Rep.* **5**, 13600 (2015).
21. Baffou, G., Polleux, J., Rigneault, H. & Monneret, S. Super-heating and micro-bubble generation around plasmonic nanoparticles under cw illumination. *J. Phys. Chem. C* **118**, 4890–4898 (2014).
22. Baral, S., Green, A. J., Livshits, M. Y., Govorov, A. O. & Richardson, H. H. Comparison of vapor formation of water at the solid/water interface to colloidal solutions using optically excited gold nanostructures. *ACS Nano* **8**, 1439–1448 (2014).
23. Bae, K. *et al.* Flexible thin-film black gold membranes with ultrabroadband plasmonic nanofocusing for efficient solar vapour generation. *Nat. Commun.* **6**, 10103 (2015).
24. Zhao, D. *et al.* Enhancing localized evaporation through separated light absorbing centers and scattering centers. *Sci. Rep.* **5**, 17276 (2015).
25. Ernst & Young Inc. *Assessment of the Local Manufacturing Potential for Concentrated Solar Power (CSP) Projects* (The World Bank, 2011).
26. Kolb, G. J., Ho, C. K., Mancini, T. R. & Gary, J. A. *Power Tower Technology Roadmap and Cost Reduction Plan* (Sandia National Labs, 2011).
27. Weiss, W., Mauthner, F. & Spork-Dur, M. *Solar Heat Worldwide* (Solar Heating and Cooling Programme, International Energy Agency, 2012).
28. Ghasemi, H. *et al.* Solar steam generation by heat localization. *Nat. Commun.* **5**, 4449 (2014).
29. Ito, Y. *et al.* Multifunctional porous graphene for high-efficiency steam generation by heat localization. *Adv. Mater.* **27**, 4302–4307 (2015).
30. Liu, Y., Chen, J., Guo, D., Cao, M. & Jiang, L. Floatable, self-cleaning, and carbon-black-based superhydrophobic gauze for the solar evaporation enhancement at the air–water interface. *ACS Appl. Mater. Interface* **7**, 13645–13652 (2015).
31. Ni, G. *et al.* Volumetric solar heating of nanofluids for direct vapor generation. *Nano Energy* **17**, 290–301 (2015).
32. Zhou, L. *et al.* 3D self-assembly of aluminium nanoparticles for plasmon-enhanced solar desalination. *Nat. Photon.* **10**, 393–398 (2016).
33. Zhou, L. *et al.* Self-assembly of highly efficient, broadband plasmonic absorbers for solar steam generation. *Sci. Adv.* **2**, e1501227 (2016).
34. Zeng, Y. *et al.* Solar evaporation enhancement using floating light-absorbing magnetic particles. *Energy Environ. Sci.* **4**, 4074–4078 (2011).
35. Zhang, L., Tang, B., Wu, J., Li, R. & Wang, P. Hydrophobic light-to-heat conversion membranes with self-healing ability for interfacial solar heating. *Adv. Mater.* **27**, 4889–4894 (2015).
36. Cao, F., McEnaney, K., Chen, G. & Ren, Z. A review of cermet-based spectrally selective solar absorbers. *Energy Environ. Sci.* **7**, 1615–1627 (2014).
37. Harding, G. L. & Zhiqiang, Y. Thermosiphon circulation in solar water heaters incorporating evacuated tubular collectors and a novel water-in-glass manifold. *Sol. Energy* **34**, 13–18 (1985).
38. Budihardjo, I. & Morrison, G. L. Performance of water-in-glass evacuated tube solar water heaters. *Sol. Energy* **83**, 49–56 (2009).
39. Schrage, R. W. *Theoretical Study of Interphase Mass Transfer* (Columbia Univ., 1953).
40. Kabeel, A. E. & El-Agouz, S. A. Review of researches and developments on solar stills. *Desalination* **276**, 1–12 (2011).
41. Velmurugan, V. & Srithar, K. Performance analysis of solar stills based on various factors affecting the productivity: a review. *Renew. Sustain. Energy Rev.* **15**, 1294–1304 (2011).
42. Cooper, P. I. The maximum efficiency of single-effect solar stills. *Sol. Energy* **15**, 205–217 (1973).
43. Lighter, S. Floating solar still. US patent no. US2820744 A (1958).
44. Miller, W. H. J. Inflatable floating solar still with capillary feed. US patent no. US2412466 A. (1946).
45. Janarthanan, B., Chandrasekaran, J. & Kumar, S. Evaporative heat loss and heat transfer for open- and closed-cycle systems of a floating tilted wick solar still. *Desalination* **180**, 291–305 (2005).

Acknowledgements

We thank D. Kraemer with help operating the solar simulator, and T. McClure and the Center for Materials Science and Engineering for the use of the FTIR. This work was partially supported by the Cooperative Agreement between the Masdar Institute of Science and Technology (Masdar Institute), Abu Dhabi, UAE and the Massachusetts Institute of Technology (MIT), Cambridge, Massachusetts, USA—Reference 02/MI/MIT/CP/11/07633/GEN/ G/00 (for the steam generation). We gratefully acknowledge funding support from the MIT S3TEC Center, an Energy Frontier Research Center funded by the Department of Energy, Office of Science, Basic Energy Sciences under Award # DE-FG02-09ER46577 (for the experimental facility). We also thank Z. Lu and E. Wang for their help in understanding the evaporation processes.

Author contributions

G.N., S.V.B. and G.C. developed the concept. G.N. and G.L. conducted the experiments. G.N., H.L., W.Y. and T.Z. prepared the models. G.N., S.V.B. and G.C. wrote the paper. G.C. directed the overall research.

Additional information

Supplementary information is available for this paper. Reprints and permissions information is available at www.nature.com/reprints. Correspondence and requests for materials should be addressed to G.C.

Competing interests

The authors have applied for a patent for this technology, but have no other competing interests.